doi:10.1246/cl.2010.493
Published on the web April 10, 2010

Highly Ordered Mesoporous α-Mn_2O_3 for Catalytic Decomposition of H_2O_2 at Low Temperatures

Jung-Nam Park,[1] Jeong Kuk Shon,[1] Mingshi Jin,[1] Seong Hee Hwang,[1]
Gwi Ok Park,[2] Jin-Hyo Boo,[1] Tae Hee Han,[3] and Ji Man Kim*[1,2]
[1]*Department of Chemistry, BK21 School of Chemical Materials Science, Sungkyunkwan University, Suwon 440-746, Korea*
[2]*Department of Energy Science and SKKU Advanced Institute of Nanotechnology, Sungkyunkwan University, Suwon 440-746, Korea*
[3]*Department of Semiconductor Systems Engineering, School of Information and Communication Engineering, Sungkyunkwan University, Suwon 440-746, Korea*

(Received February 8, 2010; CL-100130; E-mail: jimankim@skku.edu)

Highly ordered mesoporous α-Mn_2O_3 with well-defined mesopores, high surface area, and high oxygen vacancy exhibits excellent catalytic activity toward H_2O_2 decomposition at low temperature.

Recently, there has been great interest in the synthesis and application of various kinds of nanostructured transition metal oxide as an attractive alternative to traditional catalysts.[1,2] Among them, a nanocrystalline manganese oxide exhibits remarkable catalytic activities toward gas-phase oxidation of methane[3–5] and carbon monoxide,[6,7] and decomposition of NO_x.[8] The manganese oxide also shows excellent catalytic activity for decomposition of H_2O_2 compared to other transition metal oxides.[9] The decomposition of H_2O_2 in various applications, such as water treatment and bleaching using H_2O_2 in production of pulp, is desirable from an environmental viewpoint. Many researchers have also reported that various mixed metal oxides, including Mn species such as $Mn_{0.53}Fe_{2.47}O_4$,[10] CrO_3–MnO_2,[11] Li_2O–Mn_2O_3/Al_2O_3,[12] $La_{1-x}Sr_xMnO_3$[13] and $MnFe_2O_4$,[14] are active for H_2O_2 decomposition. Recently, Valdés-Solís et al. have reported that spinel ferrite $MnFe_2O_4$ nanoparticles shows much higher activity than heterogeneous catalysts previously reported in the literature.[14]

Mesoporous transition metal oxides have received enormous attention because of the unique catalytic properties attributed to high surface area and easy accessibility to active sites.[15,16] Ren et al. reported that the mesoporous metal oxides exhibit higher activity than corresponding bulk materials for low-temperature CO oxidation.[16] The high activity is related to the mesoporous structures, not just high surface area of mesoporous metal oxides. A nanoreplication method has brought forward incredible possibilities in preparing new mesoporous materials. However, the nanoreplication of mesoporous metal oxides presents some difficulty. In particular, it is necessary to carry out infiltration several times to achieve optimum loading of precursors within the mesopores.[17–19] In the present work, we have successfully synthesized highly ordered mesoporous α-Mn_2O_3 material by using a simple and facile solvent-free infiltration method.[20] The mesoporous α-Mn_2O_3 thus obtained was applied to catalytic H_2O_2 decomposition, where the catalytic performance was compared to those of bulk α-Mn_2O_3, mesoporous α-Fe_2O_3, and other reported nanocatalysts.

The mesoporous silica templates (KIT-6) were synthesized following methods reported elsewhere.[21,22] A triblock copolymer (Pluronic 123, $EO_{20}PO_{70}EO_{20}$, $M_{av} = 5800$) was used as the structure directing agent for the silica material. Tetraethylorthosilicate (Aldrich) was used as the silica source for the KIT-6 material. After calcination, the KIT-6 material was used as a template for the synthesis of α-Mn_2O_3 replica. Manganese(III) nitrate hexahydrate ($Mn(NO_3)_2 \cdot 6H_2O$, Aldrich) was used as α-Mn_2O_3 precursor. Typically, 5.0 g of the calcined KIT-6 template was heated at 100 °C for 1 h. The preheated silica template was poured into a polypropylene bottle containing 3.2 g of $Mn(NO_3)_2 \cdot 6H_2O$ (mp 37 °C) that was melted to liquid phase at 80 °C. The bottle containing the mixture was closed and shaken vigorously to mix the $Mn(NO_3)_2 \cdot 6H_2O$ and KIT-6 template. Subsequently, the bottle was put in an oven at 80 °C overnight for the spontaneous infiltration of manganese precursor within the mesopores of silica template. The composite materials then were heated to 450 °C under ambient atmosphere for 3 h. The silica template was removed by treating the composite material with 2 M NaOH solution three times. Finally, the mesoporous α-Mn_2O_3 material thus obtained was washed with distilled water and acetone several times and dried at 80 °C. Elemental analysis indicated that the amount of residual silica template was lower than 0.5 wt %. In order to compare the catalytic activity of mesoporous α-Mn_2O_3 material with other catalysts, a bulk α-Mn_2O_3 and a mesoporous α-Fe_2O_3 were also synthesized following a procedure described in the references[23,24] (See Supporting Information for details of preparation methods[25]). The H_2O_2 decomposition reactions were performed in a flask batch reactor at desired temperatures (1, 8, 18, and 25 °C) under atmospheric pressure. For typical reaction condition, the catalyst (0.05 g) was put into 31.5 mL of 0.042 M H_2O_2 solution. The effect of pH of the medium on the H_2O_2 decomposition was investigated using KOH solution instead of water. The H_2O_2 concentration depending on reaction time was measured by $KMnO_4$ titration.[26]

Figures 1a and 1b show X-ray diffraction (XRD) patterns for the KIT-6 template and the replicated mesoporous manganese oxide, respectively. As shown in the low-angle XRD pattern (Figure 1a), the KIT-6 exhibits typical XRD peaks that are characteristics of 3-D cubic (*Ia3d*) mesostructure.[27] In the case of mesoporous manganese oxide, a new XRD peak appears at a low angle as shown in Figure 1b, which corresponds to the position of the 110 reflection for *Ia3d* symmetry. Since the *Ia3d* symmetry are not allowed to have the 110 reflection, however, the presence of the new XRD peak indicates that the cubic *Ia3d* mesostructure is transformed to the tetragonal $I4_1/a$ (or lower)

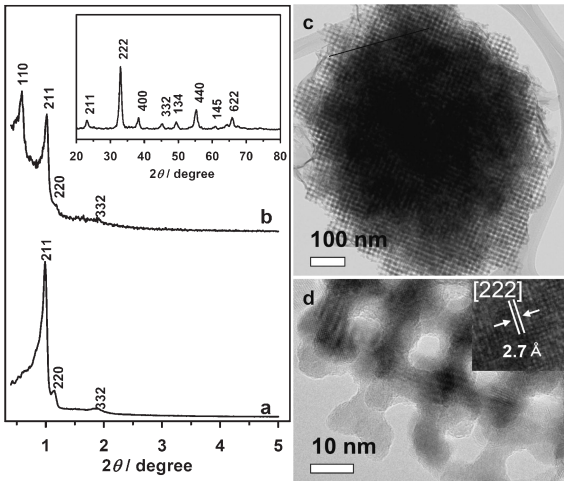

Figure 1. XRD patterns of (a) KIT-6 template and (b) mesoporous α-Mn_2O_3, and (c, d) TEM images of mesoporous α-Mn_2O_3. Insets in XRD pattern and TEM image are wide angle XRD pattern and high-resolution TEM images of mesoporous α-Mn_2O_3, respectively.

mesostructures or a single gyroid structure after the removal of silica template.[20,21,24,28,29] Very similar phase transformation upon the removal of silica template was reported for the synthesis of mesoporous carbon, metal oxides, and metals from mesoporous silica templates with cubic *Ia3d* mesostructures (MCM-48 or KIT-6).[20,21,24,28] The wide-angle XRD pattern of mesoporous manganese oxide (inset of Figure 1b) shows several peaks at 2θ; (211) at 23.08°, (222) at 32.87°, (400) at 38.14°, (332) at 45.00°, and (134) at 49.22°, which are the characteristics of α-Mn_2O_3. The average size of crystalline α-Mn_2O_3 framework is estimated to be about 10 nm by using the Scherrer formula, which is similar to the pore size of KIT-6 (ca. 7.4 nm, Figure S2 and Table S1) as well as the wall thickness estimated by TEM image (ca. 8 nm, Figure 1d). The highly ordered mesostructures of mesoporous α-Mn_2O_3 can also be confirmed by TEM images as shown in Figures 1c and 1d. A high-resolution TEM image (inset of Figure 1d) shows clear lattice fringes with the spacing of about 0.27 nm, which agrees well with the d_{222} spacing of α-Mn_2O_3. SEM images in Figure S1[25] are also consistent with the presence of highly ordered porous structures on the particle surface.

The N_2 adsorption–desorption isotherm for the mesoporous α-Mn_2O_3 gives a typical type-IV isotherm with hysteresis, which is characteristic of mesoporous materials (Figure S2[25]). A well-defined step appears in the adsorption–desorption curves around a relative pressure, p/p_0, of 0.8. As shown in Figure S2,[25] the mesoporous α-Mn_2O_3 exhibits dual porous structure (2.7 and 20 nm). The mesopore with 2.7 nm in diameter should arise from the silica framework of KIT-6 template (silica wall thickness is about 2.6 nm, Table S1[25]). The other (20 nm pore) may be generated by the structural transformation from the cubic *Ia3d* mesostructure to the others, as discussed for XRD patterns.[20,21,24,29] The mesoporous α-Fe_2O_3 and bulk α-Mn_2O_3 materials were also characterized by N_2 sorption, XRD, and SEM (Figures S2, S3, and S4).[25] The physical properties of mesoporous α-Mn_2O_3, bulk α-Mn_2O_3, and mesoporous α-Fe_2O_3 material are summarized in Table 1. The BET surface area of mesoporous α-Mn_2O_3 (118 $m^2\,g^{-1}$) shows a much higher value compared to bulk α-Mn_2O_3 (21 $m^2\,g^{-1}$). The mesoporous α-Fe_2O_3 also exhibits well-defined mesostructure and high surface area (138 $m^2\,g^{-1}$).

Table 1. Physical properties and light-off time for H_2O_2 decomposition

Sample	S_{BET}[a] /$m^2\,g^{-1}$	V_{tot}[b] /$cm^3\,g^{-1}$	Light-off time/min	
			t_{50}[c]	t_{100}[d]
KIT-6	709	0.99	—	—
Mesoporous α-Mn_2O_3	118	0.41	0.3	0.7
Bulk α-Mn_2O_3	21	0.16	1.0	10
Mesoporous α-Fe_2O_3	138	0.36	365	1380

[a]BET surface area calculated in the range of relative pressure (p/p_0) = 0.05–0.20. [b]Total pore volume measured at p/p_0 = 0.99. [c]Times when H_2O_2 conversion reaches 50% at 25 °C. [d]Times for 100% conversion of H_2O_2 at 25 °C.

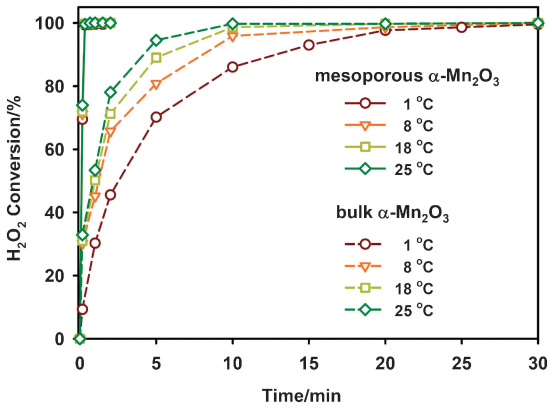

Figure 2. H_2O_2 decomposition activity over mesoporous and bulk α-Mn_2O_3 catalysts at different reaction temperatures (1, 8, 18, and 25 °C).

Figure 2 shows catalytic activity toward H_2O_2 decomposition over mesoporous and bulk α-Mn_2O_3 at different temperatures (1, 8, 18, and 25 °C), which depicts the conversion of H_2O_2. Total H_2O_2 decomposition (t_{100}) is achieved within 1 min over mesoporous α-Mn_2O_3 even at 1 °C whereas t_{100} over bulk α-Mn_2O_3 is achieved at 30 and 10 min at 1 and 25 °C, respectively. In general, H_2O_2 decomposition rate over metal oxides is known to be dependent on reaction temperature, i.e., the activity increases as the reaction temperature increases.[11,30] However, it was observed that the catalytic decomposition of H_2O_2 over the mesoporous α-Mn_2O_3 is very similar at all temperatures without any detectable difference, even at 1 °C under our reaction conditions, whereas the bulk α-Mn_2O_3 shows that the activity is highly dependent on the reaction temperatures. It is reasonable that the high activity toward H_2O_2 decomposition over mesoporous α-Mn_2O_3 at low temperature is attributed to its well-defined mesopores and high surface area.

The mechanism of H_2O_2 decomposition over transition metal oxide has been proposed by two possible reaction pathways via a surface oxygen vacancy mechanism and via radical reaction mechanism in the literature (See Supporting

Information).[10,13,25,31] The oxygen vacancies on the metal oxide surface can participate in the reaction by activating H_2O_2 to produce H_2O and O_2.[10,13] A reaction mechanism by radical formation (●OOH and ●OH) on the surface metal oxide species (for example, $Fe_{surf.}^{2+}$ and $Fe_{surf.}^{3+}$) has also been proposed.[10,31] Figure S5[25] shows H_2 temperature-programmed reduction (H_2-TPR) and O_2 temperature-programmed oxidation (O_2-TPO) data for mesoporous α-Mn_2O_3 and bulk α-Mn_2O_3 materials. As shown in Figure S5,[25] the bulk α-Mn_2O_3 exhibits two typical H_2-TPR peaks (around 360 and 470 °C),[32] whereas the mesoporous α-Mn_2O_3 exhibits broad reduction peaks below 300 °C (150 and 250 °C) in addition to the two main peaks. These additional peaks at low temperatures are probably due to the reduction of manganese species with oxygen vacancies, indicating that the mesoporous α-Mn_2O_3 has a greater number of oxygen vacant sites on the surface than bulk α-Mn_2O_3. The O_2-TPO data (Figure S5[25]) also indicate that a much larger amount of oxygen is consumed for the mesoporous α-Mn_2O_3 than bulk α-Mn_2O_3. It is reasonable that mesoporous α-Mn_2O_3 with high surface area and considerable amount of oxygen vacant sites on the surface may result in excellent catalytic activity at low temperature, where the α-Mn_2O_3 catalyst follows a surface oxygen vacancy mechanism.[13]

The activity of mesoporous α-Mn_2O_3 is compared to those of mesoporous α-Fe_2O_3 and other catalysts in the literature (Figure S6[25]) under the same reaction conditions. For comparison, the activities of $MnFe_2O_4$,[14] $Cu_xFe_{3-x}O_4$,[33] and $Mn_{0.53}Fe_{2.47}O_4$[10] catalysts reported by other authors are plotted in Figure S6.[25] Mesoporous α-Mn_2O_3 synthesized exhibits the excellent activity at low temperature compared to mesoporous α-Fe_2O_3 and other catalysts in the literature. t_{100} of mesoporous α-Fe_2O_3 is achieved in 23 h whereas the that of nanosized $MnFe_2O_4$ (BET surface area: 93 $m^2\,g^{-1}$)[14] is achieved in around 5 min. $Mn_{0.53}Fe_{2.47}O_4$ (BET surface area: 14–16 $m^2\,g^{-1}$)[10] and $Cu_xFe_{3-x}O_4$[33] exhibit relatively low activity. As shown in Figure S7,[25] the activity of mesoporous α-Mn_2O_3 is not affected by pH of the reaction medium. Moreover, there is no significant change in the H_2O_2 decomposition even though the catalyst is reused several times (Figure S8[25]). After three reaction and regeneration cycles, the XRD patterns and H_2-TPR of mesoporous α-Mn_2O_3 are very similar to those of the material before the reaction (Figure S9[25]), indicating the present mesoporous α-Mn_2O_3 is quite stable over several catalysis cycles.

In summary, the H_2O_2 decomposition activity over mesoporous α-Mn_2O_3 is considerably higher than those of bulk α-Mn_2O_3, mesoporous α-Fe_2O_3, and other nanocatalysts reported in the literature. The excellent activity of mesoporous α-Mn_2O_3 even at 1 °C is probably due to the high surface area as well as the large number of oxygen vacant sites. Moreover, the activity is not affected by reaction conditions such as reaction temperature, pH, and reutilization. From an environmental viewpoint, the present work is expected to be very useful for H_2O_2 removal applications such as water treatment or peroxide bleaching.

This work was supported by the WCU (World Class University) program through the National Research Foundation of Korea funded by the Ministry of Education, Science and Technology (R31-2008-000-10029-0). We also thank to the Priority Research Centers Program (project No. 20090094025) and the Basic Science Research Program (2009-0076903).

References and Notes

1 N. R. Shiju, V. V. Guliants, *Appl. Catal., A* **2009**, *356*, 1.
2 M. A. Carreon, V. V. Guliants, *Eur. J. Inorg. Chem.* **2005**, 27.
3 Y.-F. Han, L. Chen, K. Ramesh, E. Widjaja, S. Chilukoti, I. Kesumawinata Surjami, J. Chen, *J. Catal.* **2008**, *253*, 261.
4 Z.-C. Jiang, H. Gong, S.-B. Li, *Stud. Surf. Sci. Catal.* **1997**, *112*, 481.
5 K. Ramesh, L. Chen, F. Chen, Z. Zhong, J. Chin, H. Mook, Y.-F. Han, *Catal. Commun.* **2007**, *8*, 1421.
6 K. Ramesh, L. Chen, F. Chen, Y. Liu, Z. Wang, Y.-F. Han, *Catal. Today* **2008**, *131*, 477.
7 Y.-F. Han, F. Chen, Z.-Y. Zhong, K. Ramesh, E. Widjaja, L.-W. Chen, *Catal. Commun.* **2006**, *7*, 739.
8 M. Misono, Y. Hirao, C. Yokoyama, *Catal. Today* **1997**, *38*, 157.
9 J. T. Kohler, R. E. Altomare, J. R. Kittrell, *Ind. Eng. Chem. Prod. Res. Dev.* **1975**, *14*, 36.
10 R. C. C. Costa, M. F. F. Lelis, L. C. A. Oliveira, J. D. Fabris, J. D. Ardisson, R. R. V. A. Rios, C. N. Silva, R. M. Lago, *J. Hazard. Mater.* **2006**, *129*, 171.
11 M. M. Selim, M. K. El-Aiashi, H. S. Mazhar, S. M. Kamal, *Mater. Lett.* **1996**, *28*, 417.
12 N.-A. M. Deraz, H. H. Salim, A. Abd El-Aal, *Mater. Lett.* **2002**, *53*, 102.
13 Y. N. Lee, R. M. Lago, J. L. G. Fierro, J. González, *Appl. Catal., A* **2001**, *215*, 245.
14 T. Valdés-Solís, P. Valle-Vigón, S. Álvarez, G. Marbán, A. B. Fuertes, *Catal. Commun.* **2007**, *8*, 2037.
15 F. Schüth, *Chem. Mater.* **2001**, *13*, 3184.
16 Y. Ren, Z. Ma, L. Qian, S. Dai, H. He, P. Bruce, *Catal. Lett.* **2009**, *131*, 146.
17 S. C. Laha, R. Ryoo, *Chem. Commun.* **2003**, 2138.
18 E. Rossinyol, J. Arbiol, F. Peiró, A. Cornet, J. R. Morante, B. Tian, T. Bo, D. Zhao, *Sens. Actuators B* **2005**, *109*, 57.
19 W. Shen, X. Dong, Y. Zhu, H. Chen, J. Shi, *Microporous Mesoporous Mater.* **2005**, *85*, 157.
20 J. K. Shon, S. S. Kong, Y. S. Kim, J.-H. Lee, W. K. Park, S. C. Park, J. M. Kim, *Microporous Mesoporous Mater.* **2009**, *120*, 441.
21 J. K. Shon, S. S. Kong, J. M. Kim, C. H. Ko, M. Jin, Y. Y. Lee, S. H. Hwang, J. A. Yoon, J.-N. Kim, *Chem. Commun.* **2009**, 650.
22 S. S. Kim, H. I. Lee, J. K. Shon, J. Y. Hur, M. S. Kang, S. S. Park, S. S. Kong, J. A. Yu, M. Seo, D. H. Li, S. S. Thakur, J. M. Kim, *Chem. Lett.* **2008**, *37*, 140.
23 S. Ordóñez, J. R. Paredes, F. V. Díez, *Appl. Catal., A* **2008**, *341*, 174.
24 J. K. Shon, S. S. Kong, S. S. Kim, M. S. Kang, J. M. Kim, B. G. So, *Funct. Mater. Lett.* **2008**, *1*, 151.
25 Supporting Information is available electronically on the CSJ-Journal web site, http://www.csj.jp/journals/chem-lett/index.html.
26 M. K. Eberhardt, A. A. Román-Franco, M. R. Quiles, *Environ. Res.* **1985**, *37*, 287.
27 T.-W. Kim, F. Kleitz, B. Paul, R. Ryoo, *J. Am. Chem. Soc.* **2005**, *127*, 7601.
28 M. Kaneda, T. Tsubakiyama, A. Carlsson, Y. Sakamoto, T. Ohsuna, O. Terasaki, S. H. Joo, R. Ryoo, *J. Phys. Chem. B* **2002**, *106*, 1256.
29 H. J. Shin, R. Ryoo, Z. Liu, O. Terasaki, *J. Am. Chem. Soc.* **2001**, *123*, 1246.
30 N.-A. M. Deraz, *Mater. Lett.* **2002**, *57*, 914.
31 W. P. Kwan, B. M. Voelker, *Environ. Sci. Technol.* **2003**, *37*, 1150.
32 E. R. Stobbe, B. A. de Boer, J. W. Geus, *Catal. Today* **1999**, *47*, 161.
33 A. I. Onuchukwu, *Mater. Chem. Phys.* **1990**, *25*, 331.

